4D DIGITAL BREAST PHANTOM FOR CONTRAST-ENHANCED IMAGING

by

Dan Li

A Thesis Submitted to the Faculty of the

JAMES C. WYANT COLLEGE OF OPTICAL SCIENCES

In Partial Fulfillment of the Requirements

For the Degree of

MASTER OF SCIENCE

In the Graduate College

THE UNIVERSITY OF ARIZONA

2022

THE UNIVERSITY OF ARIZONA
GRADUATE COLLEGE

As members of the Master's Committee, we certify that we have read the thesis prepared by **Dan Li**, titled ***4D Digital Breast Phantom for Contrast-Enhanced Imaging*** and recommend that it be accepted as fulfilling the thesis requirement for the Master's Degree.

_________________________ Date: 08/08/2022
Professor Eric W. Clarkson

_________________________ Date: 08/10/2022
Professor Matthew A. Kupinski

_________________________ Date: 08/10/2022
Dr. Stephen J. Glick

Final approval and acceptance of this thesis is contingent upon the candidate's submission of the final copies of the thesis to the Graduate College.

I hereby certify that I have read this thesis prepared under my direction and recommend that it be accepted as fulfilling the Master's requirement.

_________________________ Date: 09/09/2022
Professor Eric W. Clarkson
Master's Thesis Committee Chair
Wyant College of Optical Sciences

Contents

List of Figures

Abstract

A fully simulated 4D digital breast phantom model is developed in this work. The model is based on an anthropomorphic digital breast 3D phantom, which gives the user better control of the 4D phantom features when it comes to developing and optimizing contrast enhancement imaging techniques. The fourth dimension of the phantom features different time-varying enhancement patterns for different materials including fibro glandular tissue and mass tissue. Physiological parameters that capture the key characteristics of different types of masses, for example, wash-in and wash-=out rates indicating metabolism level, are employed in the model to simulate certain fundamental features for categorizing mass types. A two-compartment model, a well-known model in the field of Pharmacokinetics, is used to depict the diffusion process of the contrast agent. Two methods are proposed to allow the simulation of the necrotic core with varying shapes.

To explore the benefit of the 4D phantom, digital mammograms are simulated and studied by the Monte Carlo method. To perform the simulation, the contrast agent blood tissue mixture's cross-section parameters are generated by linear interpolation between the parameters of blood, contrast agent, and tissue (mass or fibro glandular tissue). With the contrast agent in the tissue, higher contrast is achieved between fibro glandular tissue and mass tissue. The contrast is then further enhanced by the log scale subtraction between high and low-energy mammograms.

1 Introduction

Statistics in breast cancer, screening methods and challenges are introduced in this chapter, setting the background and necessity for the 4D phantom tool.

1.1 Breast cancer statistics

According to World Health Organization, breast cancer accounts for 12% of all new annual cancer cases globally in 2021, which makes it the most common cancer worldwide. Within the US, an estimated 287,850 new cases of invasive breast cancer are expected to be diagnosed in 2022, which will account for 30% of newly diagnosed cancers in women. Without a doubt, breast cancer posts a significant threat to women's, and sometimes men's, well-being. Therefore it is crucially important to screen high-risk people on a regular basis. However, the most significant risk factors for breast cancer are gender (being a woman) and age (getting older), which leads to a large number of screenings needed in the high-risk pool. Generally speaking, women above 40 are recommended to be screened for breast cancer on a regular basis. While we see the majority of breast cancers happens above 40 years old, it is not rare to see cases at younger age. Typically, other than the age and gender factors, women with dense breast tissue or a close family history of breast cancer are also at higher risk.

1.2 Challenges in screening breast cancer

The most popular screening method for breast cancer is a mammogram, which is an X-ray picture of the breast. According to the FDA, more than 40 million mammograms are performed per year in the US. Other than mammograms, another emerging technology, digital breast tomosynthesis(DBT) is also getting more and more common in the diagnosis of breast cancer by providing a synthesized 3D reconstruction of the breast using limited angle X-ray projection. DBT has been proved to have a higher detection rate of breast cancer compared to mammograms while also requiring a higher radiation dosage. With limited angle projections, the 3D reconstruction acquired by DBT has its limitations. Dedicated breast computed tomography (breast CT) has been implemented to address the limitations.

However, the improvement in detection rate of cancerous masses is limited by the nature of the similarity between the attenuation coefficients of fibroglandular tissue and cancerous tissue. Due to this similarity, there are two primary challenges. The first difficulty is detecting a tumor in dense breast tissue. Breast tissue is composed of milk glands, milk ducts, supportive tissue, and fatty tissue. Dense breast tissue refers to the first three components, which have higher densities and attenuation coefficients than fatty tissue. With a higher attenuation coefficient, more X rays get absorbed in the tissue, hence they are brighter in the mammogram. While the fatty tissue has a lower density and attenuation coefficient, therefor it is considered a non-dense breast tissue. Figure 1 is an example of different levels of dense breast tissue. The level of breast density is increased from left to right in the figure, correspondingly the white solid area is enlarged as well.

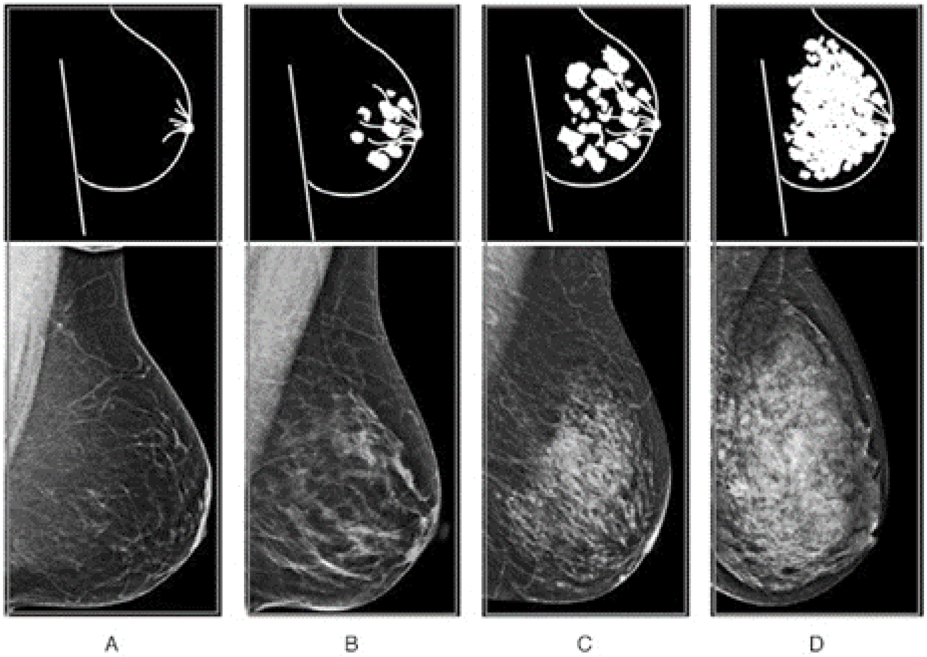

Figure 1: Different levels of dense breasts

Non-dense breast tissue appears black and transparent on a mammography. As illustrated in Figure 2, dense breast tissue appears as a solid white and bright area, making it difficult to see through and notice the mass. As illustrated by the figure, while a larger mass exists on the right side of the figure, it is harder to spot the mass due to the bright background caused by dense breast tissues.

The second challenge is to determine the malignancy level of the mass. Among 40 million mammograms performed per year, more than 1 million are followed with breast biopsies. Only 20 percent of those biopsies yield a diagnosis of breast cancer, which means 80 percent of those procedures may have been unnecessary. The similarity of the attenuation coefficients

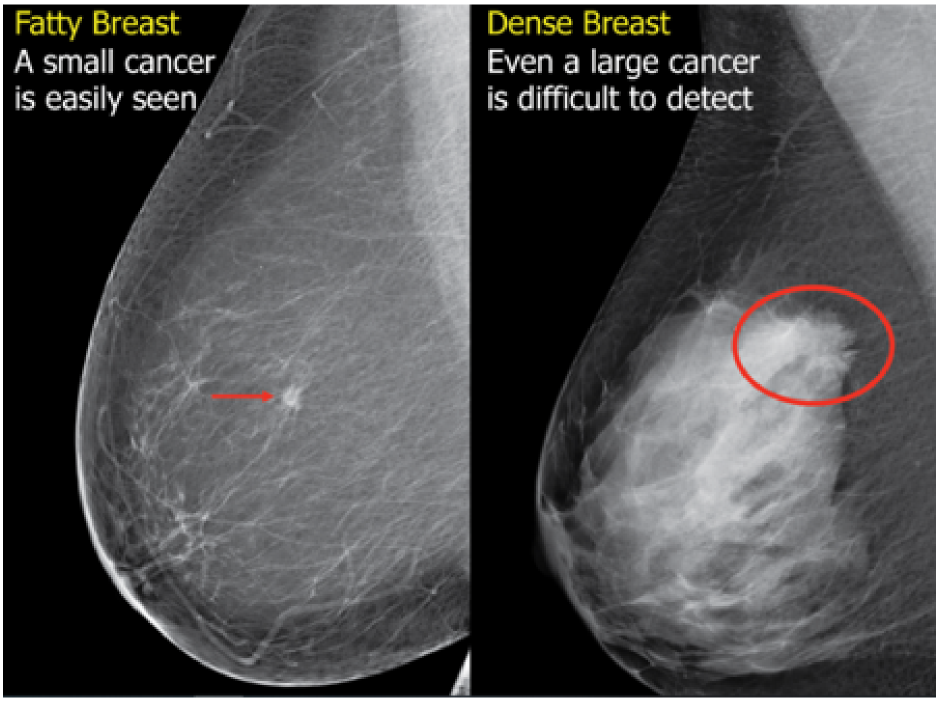

Figure 2: Cancer detection in dense breast vs non-dense breast

between malignant mass tissue and benign mass tissue again explains the difficulty in categorizing malignant tumors. Figure 3 is an example of different types of masses in mammograms. We can get a feeling of the difficulty in differentiating them through the this figure.

1.3 Tools developed

To address these challenges, fundamental characteristics need to be explored. We know that different types of tissue have different metabolism. When it comes to absorption of a contrast agent, fibro glandular tissue, malignant mass tissue, and benign mass tissue vary a lot. The differences in metabolism can be exploited by injecting contrast agents, for example, iodine-based con-

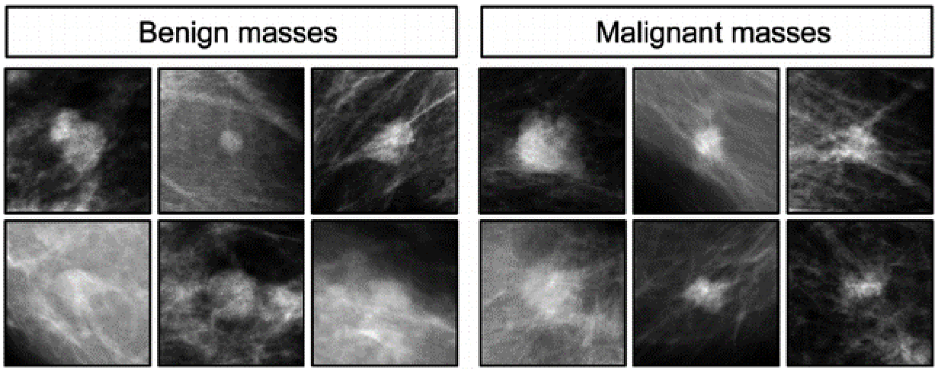

Figure 3: Benign masses vs Malignant masses

trast agents. As iodine has a high atomic number, 53, compared to most tissues in the body, the administration of iodinated material produces image contrast due to different attenuation coefficients, which helps the radiologists detect and categorize cancerous tumors. This technology is termed contrast-enhanced imaging.

Over the last few decades, there has been a lot of research and practices focusing on this topic to image the microvasculature in tumors. To further develop and optimize the contrast-enhanced breast imaging technique, tools are needed to simulate and analyse the diffusion process of the contrast agent in the breast tissue. Here we propose a 4D phantom that can be used to simulate contrast-enhanced breast imaging and optimize the detection and categorisation of breast tumors. The phantom is fully digitized, therefore easy to use. It is introduced in the second chapter. Based on the 4D phantom developed here, in the third chapter, the Monte Carlo simulation method is used to generate mammograms at different time points to demonstrate different diffusion processes and contrast enhancement results for different masses. Dual-energy mammograms are also explored with a log scale subtraction method. In the fourth chapter, the background of the mass is reduced through dual-energy subtraction method, and we show the potential for enhancement of masses.

2 4D Digital Breast Phantom

This chapter starts by introducing the 3D digital phantom used for the 4D diffusion model, where the fourth dimension is time, characterizing the change of contrast agent concentration level with respect to time itself. The fourth dimension provides the bases for the dynamic process. This work is expanding on a previous model[1]. Here we use a digital anthropomorphic phantom instead of a patient-based phantom. With the knowledge of artery locations and the two-compartmental model, a more realistic diffusion model can be achieved. The necrotic core is also modeled with two approaches.

To model the diffusion process, certain assumptions are established. The initial assumption is that the contrast agent carried from the artery is the only source of contrast agent for all tissues. This assumption indicates the independence of contrast agent concentration levels between all tissues except for artery tissue since the artery is the only source. For example, a fibro glandular tissue voxel's concentration level is not influenced by the nearby fibro glandular tissue or mass tissue. The association between voxels that are indexed by the same type of tissue ID is described by the second assumption. Here we assume the time enhancement patterns are the same for the same type of tissue, though randomness is introduced by randomizing some physical parameters (the blood flow value) with respect to a certain mean to generate minor fluctuation. Since the model is linear, it yields similar results between adding noise to the blood flow and to the final concentration level of the contrast agent as long as the same distribution is followed. The last assumption is natural after the first two assumptions. With the artery being the only source of contrast agent and voxels of the same tissue type sharing the same enhancement patterns, it is fair to assume that the major differences in enhancement patterns come from the tissue type and location with respect to the artery voxel. With those three assumptions, the 4D diffusion model is further explained in the following sections. Starting with the 3D digital breast phantom, we build the previous three assumptions into the final 4D phantom.

2.1 3D digital breast phantom

The 3D digital breast phantom adopted here was implemented by Christian G. Graff in 2016[2]. This phantom is made available as a free open source project through GitHub.

This digital phantom generates random voxelized breasts by simulating the distribution of different breast tissue structures. Parameters can be changed to achieve arbitrary resolution. To be specific, the author creates the phantom in an agnostic manner. Those voxels in the digital breast phantoms contain the features that are crucial to breast imaging and capture the variability of those features found in the patient population. Each voxel in the model is labeled by a single type of tissue. Skin, nipple, lactiferous duct, terminal duct lobular unit (TDLU), inter-lobular glandular tissue, fat, the suspensory ligaments of Cooper, chest muscle, artery, and vein are all modeled and simulated in the phantom. The breast shape in the model is also quite realistic. These simulated breasts can be used for a variety of applications. With knowledge of the label of each voxel, we can develop different diffusion models for different tissues. Figure 4 is an example of the mammogram of the generated 3D phantom.

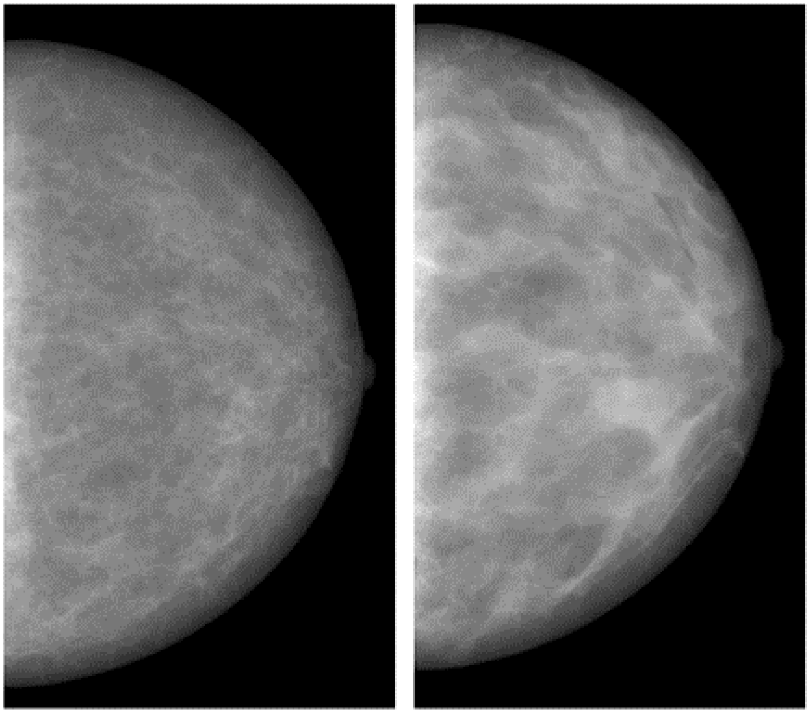

Figure 4: mammographic projections of a fatty breast (10% glandular volume) left, and moderately dense breast(30% glandular volume)right generated via ray tracing

Abnormal tissue types (malignant and benign masses, calcifications, etc.) are not considered in Graff's phantom. Here in this work we focus on the modeling the uptake of iodine (representing the contrast agent) in different masses. The mass model we adopted here is from another paper written by Sisternes[3]. In the paper a modified stochastic Gaussian random sphere model was used to construct the core tumor mass, and an iterative fractal branching technique was used to add random spicule features to the simulated 3D breast masses. Digital mammograms were used to verify the quality of simulated masses in the paper. Both experienced radiologist readers and computer-aided diagnosis (CAD) tools are used as observers to see if there were any significant discrepancies between the genuine and hybrid pictures. It was proved that there is no significant difference between the genuine and hybrid mammograms after the two observer tests.

The mass generated is added into Graff's phantom simply by replacing the label of current voxel with the label of mass. The location of insertion is chosen randomly. Several mass samples are provided in the following Figure 5 to give a feeling of the mass generated.

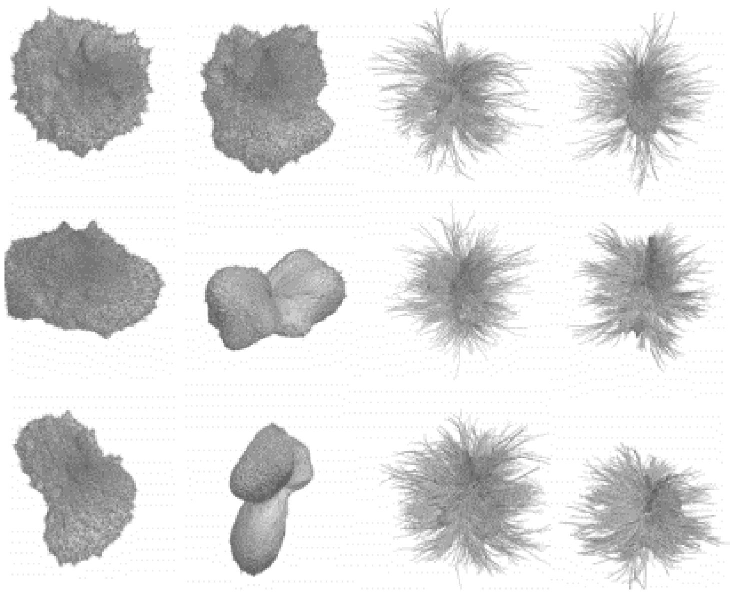

Figure 5: Different masses: left six lobular masses, right six spiculated masses

2.2 Diffusion model

As mentioned earlier, three assumptions are made to develop the 4D model. The first assumption describes the source of contrast agent available to all tissues. This assumption implies the independence of contrast agent concentration levels in all tissues with the exception of arterial tissue. The second assumption describes the relationships between voxels that are indexed by the same type of tissue ID. Excluding the effect of minor randomness introduced, we presume the time enhancement patterns are the same for the same type of tissue. After the first two assumptions, the final assumption is natural. Given that the artery is the only source of contrast agent and that voxels of the same tissue type have similar enhancement patterns, it's reasonable to believe that the significant changes in enhancement pattern are due to tissue type and placement relative to the artery voxel.

With those assumptions, the diffusion process for each voxel is modeled in two steps. The first step describes the time delay for each voxel before the tissue represented by the voxel ID starts responding to the injection of contrast agent, while the second step describes the change of concentration level of contrast agent in a certain type of tissue. To be specific, the injection of a contrast agent in the artery is treated as input of the diffusion process for each tissue. The time delay for each voxel is referenced to the start of injection, and the injected contrast agent itself can be modeled by an arterial input function (which will be introduced in the following section) to serve as the numerical input for the future uptake process. While the change of concentration level of contrast agent (iodine uptake process) for each type of tissue is different due to different characteristics of the certain type of tissue, for the same type of tissue, the change of concentration level is more or less the same except that the timing of onset of each process is different due to the relevant distance to the artery tissue. We do add randomness for different voxels by adding Gaussian noise to the blood flow value (introduced in the following section), but it only serves as noise. Figure 6 is a simple diagram for the modelling process.

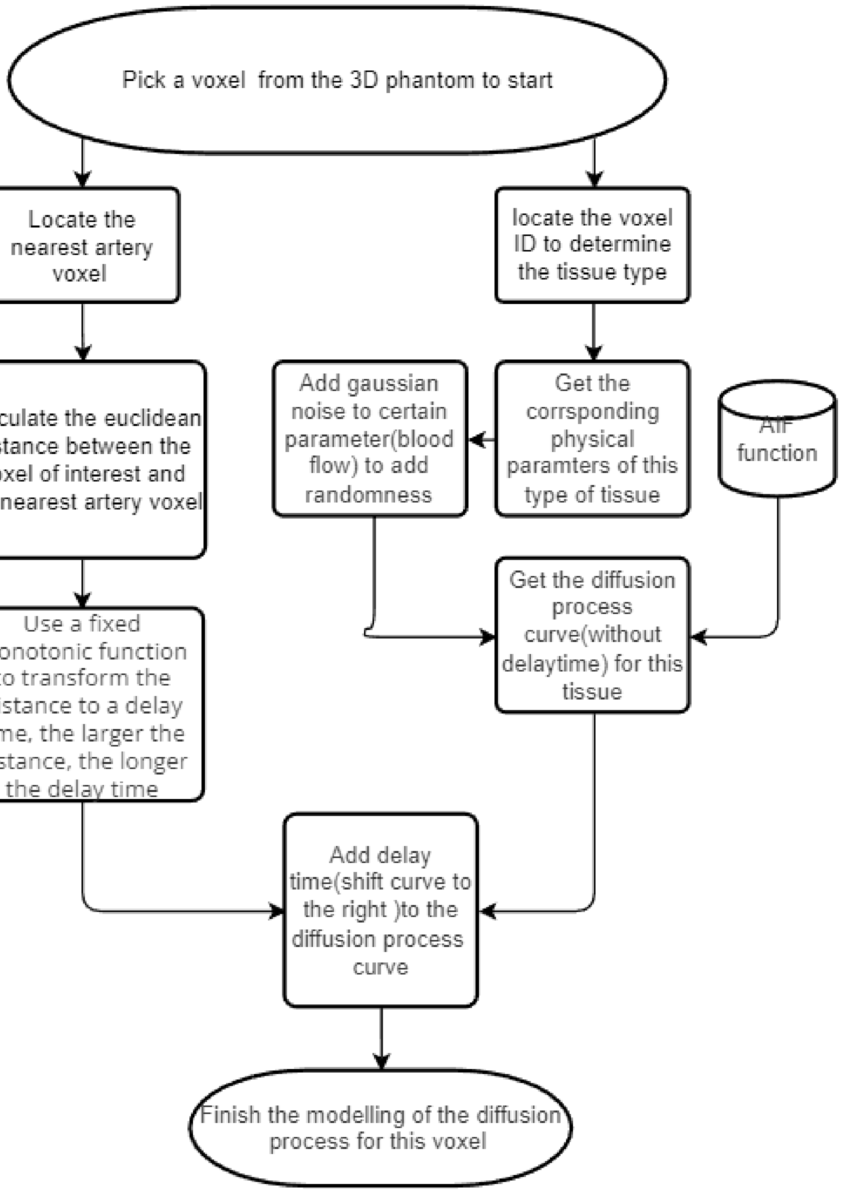

Figure 6: Diffusion process modelling for a single voxel, the left branch describes the first step, the right branch describes the second step.

The first step is mainly described in the left branch, details described here will be further explained in the following sections. The second step is represented by the right branch in the diagram. The next section will provide additional explanations for the details presented here.

2.3 Time delay model

It takes two steps for the contrast agent to reach a certain voxel of tissue in the breast. First, the contrast agent arrives in the artery in the breast after the injection. Since arterial blood flow velocities range from 4.9 to $56cm/sec$[4][5], it is fair to assume the contrast agent arrives in all artery voxels at the same time.

As soon as the contrast agent arrives in the artery voxel within the breast, the diffusion process kicks in. Ideally, all of the artery voxels should have an influence on the nearby tissues. It is hard to define nearby quantitatively and model all the influences between every voxel. Previous literature tried to model this procedure by picking two source voxels on the chest wall and then using exponential decay functions to approximate the time spent to travel from the two source voxels to a certain voxel of tissue. In our phantom, there are more than 70 thousand voxels simulating the artery tree. If a similar approach is utilized, the computation would be extremely time consuming just to calculate the delay time for each voxel. We can implement the algorithm using a parallel computation technique, or another modeling method can be implemented to qualitatively achieve similar results.

Here we calculate the Euclidean distance of each voxel to its nearest artery voxel, then use this distance as the exponent in an exponential decay function. Figure 7 is a 2D picture of the maximum projection of the artery from our 3D phantom and its corresponding delay map that shows the Euclidean distance to its nearest artery voxel.

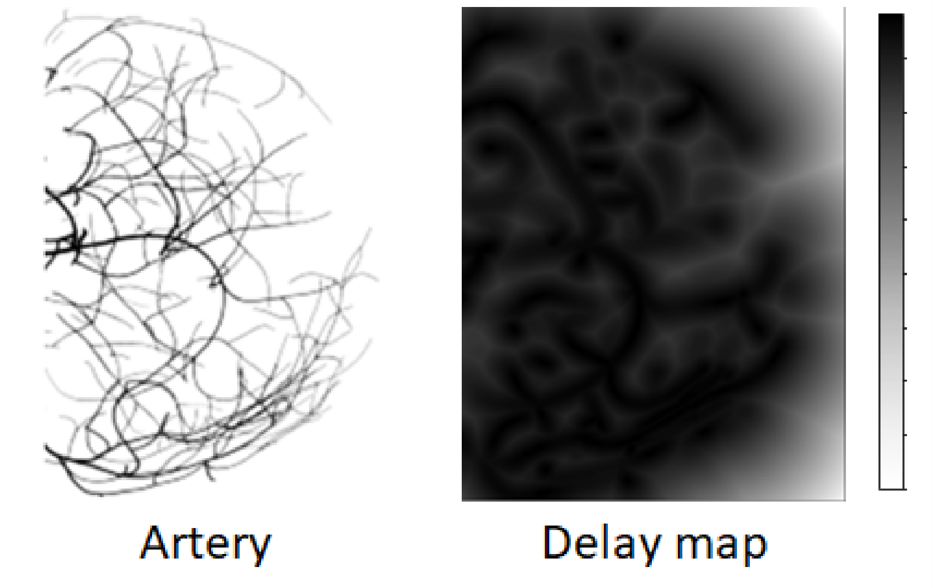

Figure 7: Maximum intensity projection of the artery tree in the 3D phantom, and the contrast agent delay map.

The delay time for each voxel is computed according to the following equation:

$$DT(x, y, z) = [1 - exp(-\frac{\sqrt{((x - x_i)^2 + (y - y_i)^2 + (z - z_i)^2)}}{R})] * T \quad (1)$$

Where the index i for the specific artery voxel ID is chosen such that it has the smallest Euclidean distance to the voxel of interest.

$$i = \arg\min_i \sqrt{((x - x_i)^2 + (y - y_i)^2 + (z - z_i)^2)} \quad (2)$$

Here the i under argmin in the previous equation indicates each index of all the artery voxels. R in equation 1 is a parameter modeling the spatial distribution of the time delay among all the voxels. T in equation 1 specifies the maximum time delay for all of the voxels. In general, the further away from the artery voxel, the longer the delay time, which is the qualitative result we aimed for at the beginning.

2.4 Diffusion process for mass tissue

The key component of this 4D phantom is to model the diffusion processes of different types of masses, so we can differentiate between the benign and malignant masses. This section starts by introducing relevant physiological parameters and models needed to simulate the iodine uptake process in the mass, then the final model for the diffusion process in the mass is proposed and implemented.

2.4.1 Parameters and models

Before diving into the model, some physiological input parameters for the 4D breast phantom are discussed. The physiological meaning of those parameters will be discussed as well. The numerical values we adopted in this work are displayed in the following Figure 8. BF (blood flow) describes the amount of blood entering and also exiting from a certain volume of tissue, the unit is in mL /min/ 100 mL. Higher metabolism normally indicates higher blood flow values. Both the mean and variance are provided for the blood flow. The average time, in seconds, that blood cells spend within a given volume of capillary circulation in a certain tissue is referred to as mean transit time (MTT). Both BF and MTT can be evaluated as part of the CT and MR perfusion protocols.

	Blood flow ($\overline{BV} \pm V_{BF}$)(mL/min/100 mL)	Mean transit time (MTT) [s]	Wash-in polynomial grade (R_{washin})	Wash-out polynomial grade ($R_{washout}$)
Fibroglandular tissue	7.15 ± 0.1	71.3 ± 1.8	Not defined	Not defined
Malignant Lesion model	70.3 ± 0.3	30.3 ± 0.4	5	3
Benign lesion model	14.8 ± 0.3	62.4 ± 2.5	1.25	2

Figure 8: Physiological input parameters with values adopted in this work

The wash-in rate is the highest slope on the time intensity curve between the time of onset of contrast inflow and the time of peak enhancement. This parameter in each voxel can be automatically determined using DCE-MR data sets[6]. A radiologist would calculate the wash-in rate value in four different regions of interest (ROIs) : over cancer tissue, normal tissue in the peripheral zone, normal tissue in the inner two-thirds of the transitional zone, and normal tissue in the outer third of the transitional zone. The same goes for wash-out rate. Both wash-in rate and wash-out rate are physiological parameters indicating the metabolism of the mass.

Other than physiological parameters, two models are referenced to implement the final simulation of the uptake process. The first model is the arterial input function. It is defined as the concentration of the contrast agent in an artery measured over time by focusing on a region of interest. It is used here to quantitatively define numerical values of the injection of the contrast agent. The arterial input function we used is shown in Figure 9. Here the maximum peak for the concentration of iodine-based contrast agent is 10 mg/ml, which is qualitatively consistent with measurements in clinical experiments. The span is about 30 seconds, it is also quite realistic considering the injection process.

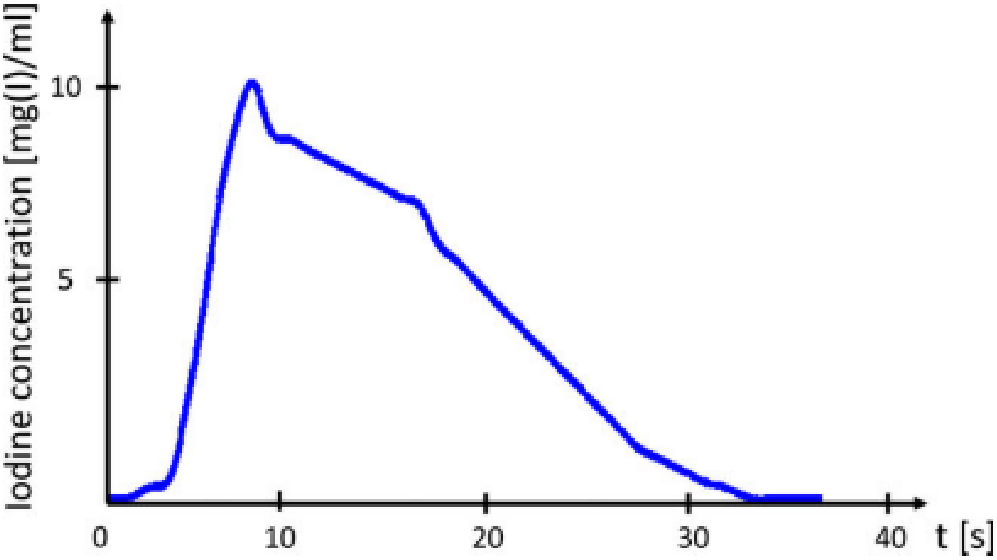

Figure 9: Arterial input function adopted in this work

2.4.2 Two compartmental model

Another model we referenced here is a two compartmental model. It is a well-known model in the field of Pharmacokinetics[7].

Pharmacokinetics is a scientific subject that underpins the application of medicines. Medicine is normally chosen using an evidence-based clinical practice approach. Pharmacokinetics principles must be applied to guarantee that the right drug is chosen for the right route of administration. The dosage regimen for the treatment in a given patient can be determined based on the patient's drug handling parameters, which require an understanding of absorption(A), distribution(D), metabolism(M), and excretion(E). A mathematical basis is provided by pharmacokinetics to assess the time course of drugs. It enables all of those four processes (ADME) to be modeled quantitatively.

The scenario of pharmacokinetics is quite similar to the diffusion process of contrast agents. When it comes to modeling the concentration level of iodinated contrast agents, as in the field of pharmacokinetics, all four processes, absorption, distribution, metabolism, and excretion needs to be taken into consideration. The final model will be able to depict the fate of the contrast agent after it has been injected.

There are two different hypotheses about the body. In certain scenarios, the body can be described as a kinetically homogeneous object. Following this assumption, the medicine will reach instant equilibration once being administrated or injected. Normally most drugs used in clinical practice show first-order reaction, meaning the rate of elimination of drug A is described as the following:

$$\frac{dA}{dt} = -kA \tag{3}$$

With the one compartment model assumption, the concentration level of drug A should be similar to what is showed in Figure 10.

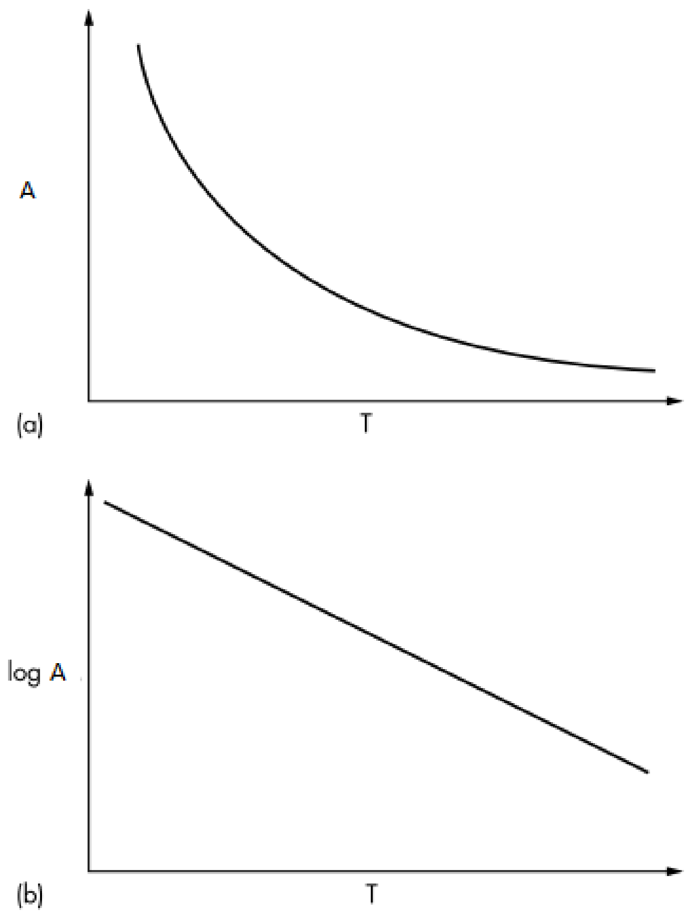

Figure 10: (a) concentration level of A versus time profile of a drug in a one-compartment model.(b) concentration level of A in log scale versus time profile of a drug in a one-compartment model

Unlike the homogeneous object assumption in the one-compartment model, The two-compartment model breaks the body into two parts: a central compartment and a peripheral compartment. Though there are no physiological functions or anatomical meaning for the two compartments, a common practice is to assume the central compartment as highly perfused tissues such as the heart, lungs, kidneys, liver, and brain. In the case of our breast phantom, it would be the artery. The peripheral compartment is normally the less well-perfused tissue, such as muscle, fat, and skin. In our model, we assume everything else is peripheral compared to the artery, which is a reasonable assumption.

With a two compartment model, the drug or contrast agent, does not reach instant equilibration between the two parts. Instead, there is a dynamic process following up as showed in Figure 11.

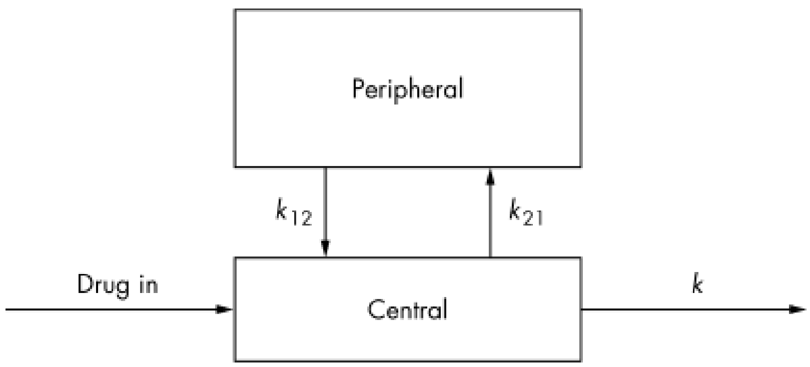

Figure 11: All the k values in the diagram are rates of transfer as in the previous equation describing first-order reaction.

Assuming all of the transfer rates (absorption, elimination) are first-order reactions. The changing rate of the contrast agent can be represented as:

$$\frac{dX_c}{dt} = -k_{12}X_c + k_{21}X_b \tag{4}$$

$$\frac{dX_b}{dt} = -kX_b + k_{12}X_c - k_{21}X_b \tag{5}$$

All of the K values in the equation 4 and equation 5 are consistent with the diagram shown earlier in Figure 11. X_c and X_b refer to the concentration level in the central part and peripheral part. Solving for these two equations, we get the concentration level in the peripheral compartment as follows:

$$X_c = \frac{X_0 k_{21}[exp(-k_{12}t) - exp(-k_{21}t)]}{k_{21} - k_{12}} \tag{6}$$

Based on this two-compartment model and other physiological parameters, we establish the following model for the contrast agent uptake in the mass tissue:

$$TEC(x_0, y_0, z_0, t) = AIF(t) * Wash(t|x_0, y_0, z_0) \cdot BF_m \tag{7}$$

$$Wash(t|x_0, y_0, z_0) = \frac{X_0 k_a (exp^{(-k_e t/R)} - exp^{(-k_a t/R)})}{k_a - k_e} \tag{8}$$

Where TEC represents the time enhancement curve, which describes the intensity of iodine uptake as a function of time for a voxel representing mass tissue. AIF represents the artery input function, and the Wash function describes the process of absorbing and eliminating dynamics. The AIF is convolved with the wash function to give a quantitative measurement of the uptake intensity. Here our wash function is a two-compartment model. The artery is viewed as a central compartment due to its feature of being highly perfused. The mass tissue is assumed to be the peripheral compartment, since it is less perfused compared to the artery. We use the wash-in and wash-out rates to quantitatively model the rate of absorption and elimination, which is reasonable due to a similar physiological foundation. Another parameter R is used for properly adjusting the model to match different clinical scenarios. In the final TEC curve, R here gives control to the time span of the diffusion process. A bigger R will lead to a wider time range of the whole procedure, meaning a longer time for the fate of the contrast agent to be determined. X_0 gives control to the scaling of the concentration level. Different wash-in and wash-out rates are normally found in different tumors. With those two rates ingrained in the model, different TEC functions can easily be achieved, hence different enhancement patterns. The time enhancement curve for three different tissues is displayed in Figure 12.

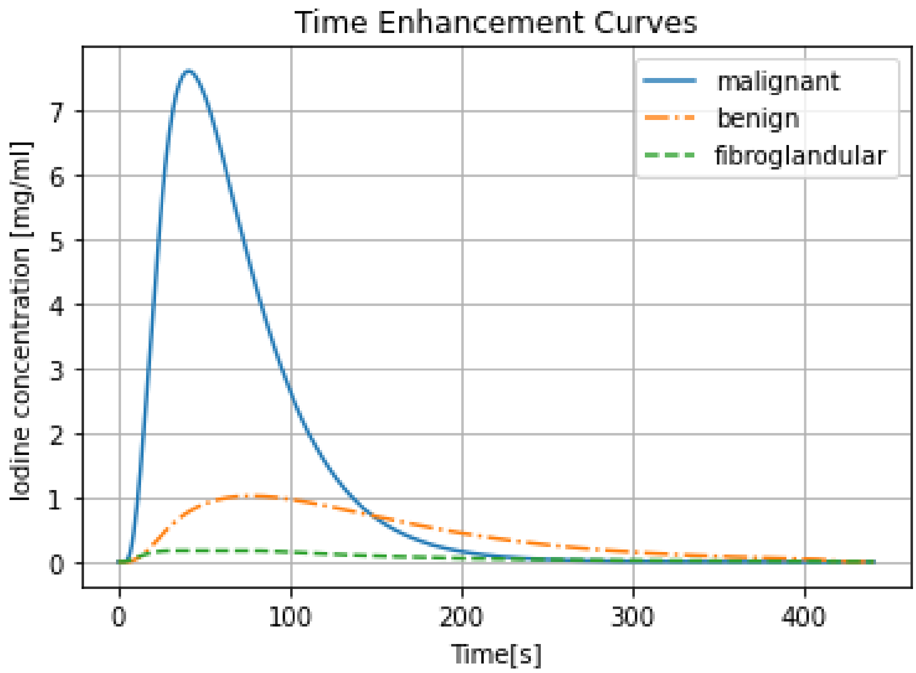

Figure 12: Time enhancement curves for malignant tumor tissue, benign tumor tissue, and fibro glandular tissue. There is no time delay assigned, in an actual time enhancement for a certain voxel of tissue, the corresponding curve of this certain type of tissue should be shifted to the right for the delayed time assigned to the voxel given its distance to the nearest artery voxel

The peak value for malignant and benign masses is controlled by the same set of parameters. It is qualitatively consistent with clinical observations. However, there are few references for the peak value for the fibro glandular

TEC curve, and a lot of literature ignores the uptake of fibro glandular tissue. The model of fibro glandular tissue uptake process is described in the following section.

2.5 Diffusion process for fibro glandular tissue

Wash-in and Wash-out rates are generally not measured in clinics for fibro glandular tissue. Another approach is used to model this type of tissue. To calculate the time enhancement curve associated with a fibro glandular voxel, we need to convolve the AIF function with an attenuated blood flow function. Here the blood flow function is formed by adding an exponential decay function after a mean-transit time. The mathematical model is described as follows:

$$TEC(x_0, y_0, z_0, t) = AIF(t) * BF(t|x_0, y_0, z_0) \tag{9}$$

$$BF(t|x_0, y_0, z_0) = \begin{cases} BF_f, t < MTT \\ BF_f \cdot e^{-(t-MTT)/R}, t \geq MTT \end{cases} \tag{10}$$

Here R in equation 10 is a parameter to control the exponential decay rate, so different time spans of the process can be achieved. We set R to be 100 and the following TEC function (Figure 14) is achieved. The blood flow function is also provided in Figure 13. BF_f here refers to the mean blood flow value for the fibro glandular tissue.

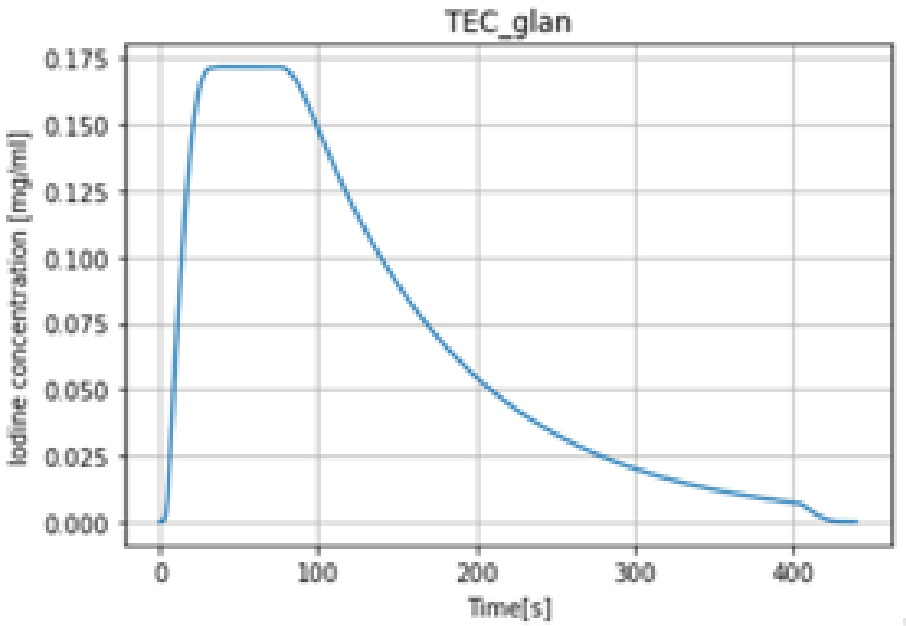

Figure 13: Time enhancement curves for fibro glandular tissue. There is no time delay assigned, in an actual time enhancement for a certain voxel of tissue, the corresponding curve of this certain type of tissue should be shifted to the right for the delayed time assigned to the voxel given its distance to the nearest artery voxel.

2.6 4D phantom

With the time delay model and TEC models built, the final 4D phantom can be established.

We start in a single voxel and model how the iodine concentration level changes with respect to time. For each voxel, to know its iodine uptake level at a given time, there are four steps needed.

First, identify the corresponding tissue type of the voxel. Here we only recognize three different types of tissues: artery tissue, mass tissue and fibro

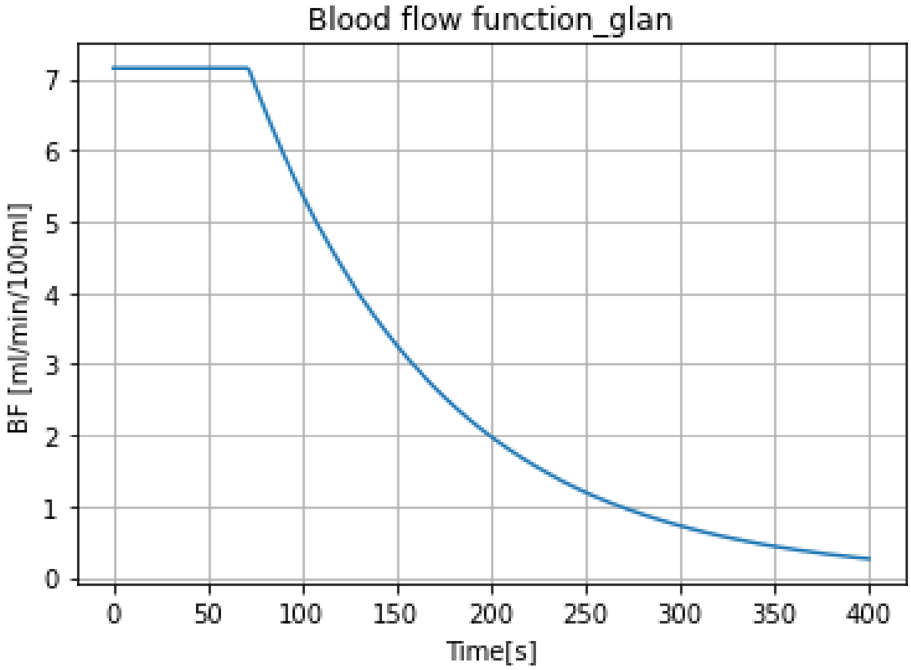

Figure 14: Blood flow function according to equation 10, here R is also set as 100.

glandular tissue. With this information, we will know the time enhancement curve of this voxel without time delay. For an artery voxel, the time enhancement curve is the same as the artery input function considering the speed of travel within the artery. No time delay is assumed for artery tissues. In this model, we assume there is no iodine uptake in any other tissues, which include: fatty tissue, skin, nipple, lactiferous duct, terminal duct lobular unit (TDLU), inter-lobular glandular tissue, the suspensory ligaments of Cooper, and chest muscle.

Then, the corresponding delay time is calculated from equation 1 after finding the voxel of the artery that has the smallest Euclidean distance to this voxel of interest.

The third step involves shifting the time enhancement curve to the right by the amount of time specified by the delay function. We could also add randomness at this step by adding Gaussian noise, which will be explained further in the next subsection. At this moment, randomness is not introduced, so we have a clear picture of the main components.

The last step will be finding the intensity of the iodine uptake at a certain time using the shifted time enhancement curve in this certain tissue type. The previous four steps can be repeated for all of the voxels of interest at a certain desired time, a time slice of the 4D phantom will be achieved this way. Repeating the whole procedure for all time frames needed for a 3D video, a final 4D phantom will be established.

The whole process is illustrated in the following Figure 15. Again, this process only focuses on one voxel.

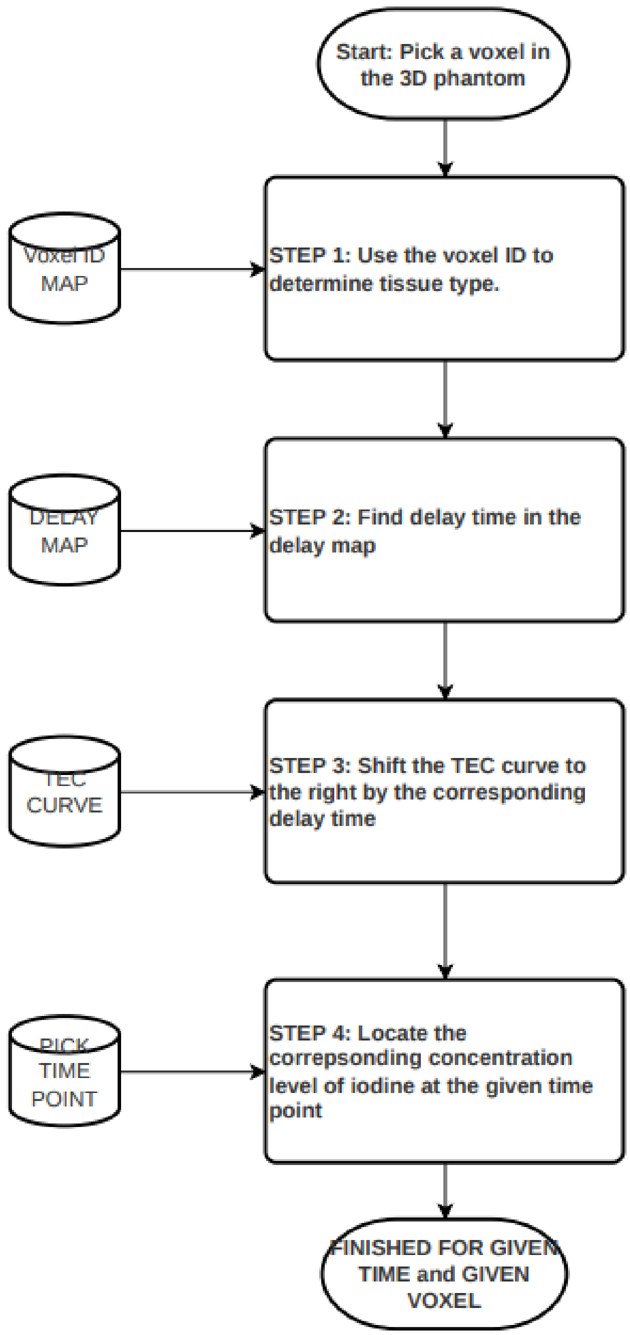

Figure 15: The diagram only shows the 4 steps to model a single voxel's iodine concentration level at a given time, to get a full 4D phantom. We repeat this process for all given times and all voxels in the original 3D phantom

Using the steps described in the diagram, and repeating them for all voxels in the central slice of the 3D phantom, a series of time slices of the 4D phantom can be constructed. In Figure 16, we can see a big tumor with the index 200 in middle of the phantom. For display purpose, only the central slice of the 3D phantom is displayed. The tumor size is chosen to be quite big, so the pattern of enhancement of the mass can be observed closely.

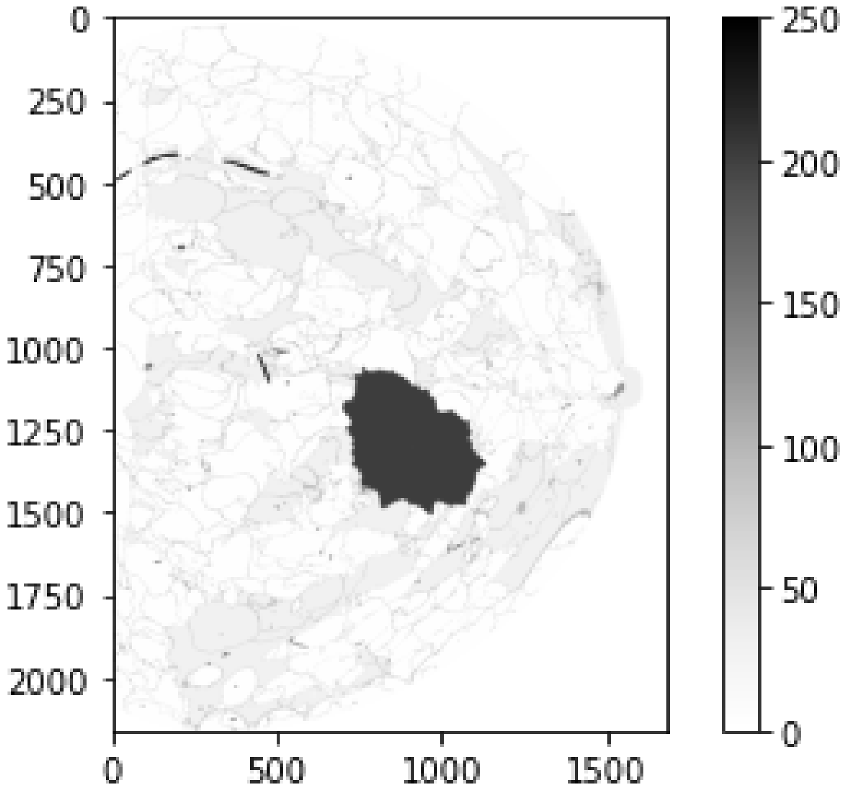

Figure 16: Central slice of the 3D phantom, the intensity of each voxel is represented by the index indicating the tissue type of this voxel. Here fibroglandular tissue is indexed by 29, tumor tissue is indexed by 200, artery also has a high index which is 150, the dark lines in the figure are artery voxels. The round dark spot in the middle is our tumor.

In the experiment, R is specified to be 100 in the model. It can be adjusted to achieve different time spans. In the following Figure 17, the tumor is modeled twice, each as malignant and benign using the corresponding physiological parameters listed in Figure 8. Here figure (a) is the central slice of the 3D phantom, figure (b) is the enhancement curve for different tissues. The first two figures give a reference for the following. Figure (c) shows a series of time points for a benign tumor, and figure (d) shows a series of time points for a malignant tumor. Different enhancement patterns can be observed by comparing the last two figures. while the malignant tumor has an enhancement pattern with a higher peak value, the benign tumor has a longer enhancement period. This can be further explored using the MCGPU Monte Carlo simulation and Dual-energy contrast-enhanced imaging, this topic will be further introduced in the next chapter.

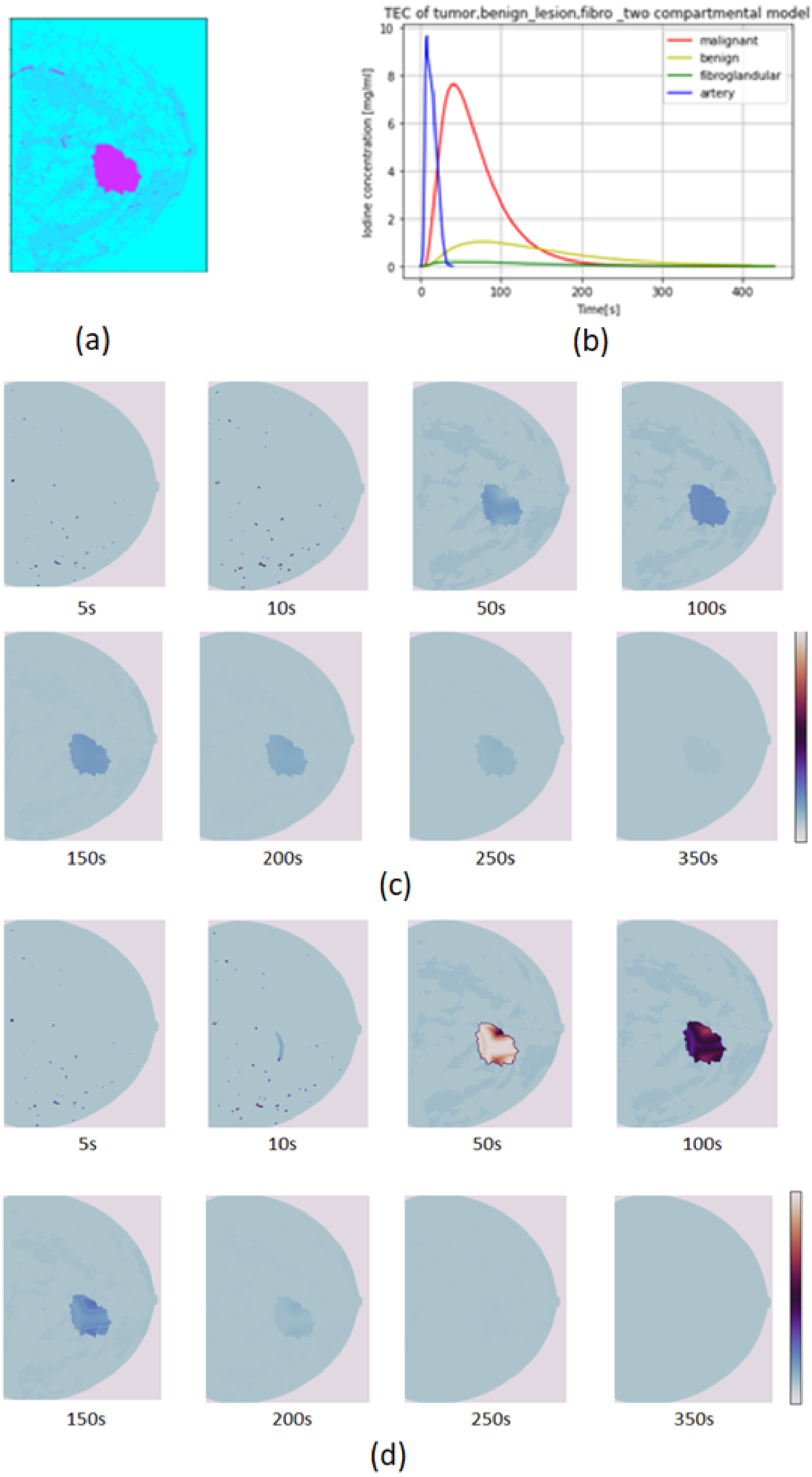

Figure 17: Central slice of the 4D phantom in different time points: (a) the central slice of the 3D phantom; (b) enhancement curves for different tissues; (c) a series of time points for benign tumor; (d) a series of time points for malignant tumor.

2.6.1 Randomness

There is no randomness introduced so far in our model, which is not realistic. Though the same type of tissue normally shows similar patterns, there could be a variation due to heterogeneity. This variation can be introduced by perturbing the blood flow parameter. Basically, as with the parameter illustrated in figure 8, we choose a mean for our blood flow value, then introduce the perturbation using the random variation as described in the following equation 11

$$BF(x, y, z) = \bar{BF} + N(x, y, z) \tag{11}$$

Here N is a Gaussian random variable with zero mean and the same variance as desired for BF. Due to the linearity of the model, a similar effect can be achieved by adding randomness in the TEC curve directly. The variance of the Gaussian random variable needs to be scaled accordingly.

With the randomness factor, a time slice of the 4D phantom was created as a comparison to the one without randomness, and it is displayed and compared in the following Figure 18. Due to the small variance introduced, the noise level is quite small.

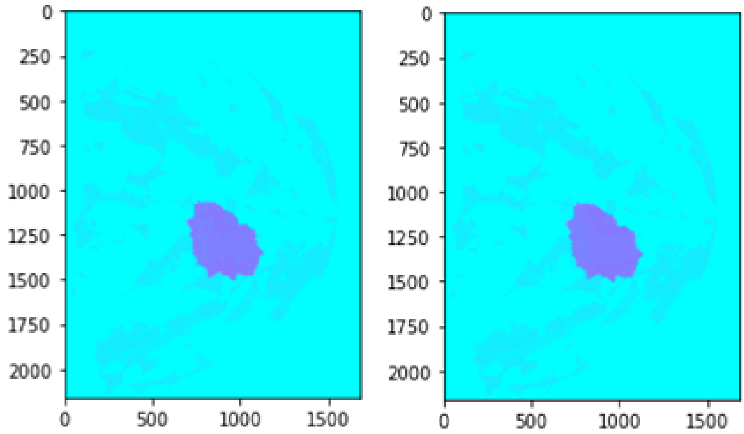

Figure 18: Central slice of the 4D phantom, left one modeled randomness, the right one is a central slice without randomness

2.6.2 Necrotic core

Another special case considered in 4D the phantom is the necrotic core. Necrotic cores are formed from the combination of apoptosis of advanced lesional macrophages and defective phagocytic clearance (or efferocytosis) of the apoptotic macrophages in advanced plaques. In plain words, a tumor can be half dead inside or at a certain portion in the tumor, which will lead to heterogeneity in the enhancement pattern. This effect is noticed in clinics when there are two types of cancer present in one mass. With certain treatments, one of two cancers can be susceptible to the treatment plan while the other one is not. This will lead to mass with a hollow core (or a partial dead mass).

To allow this varied breast tumor enhancement pattern, a 3D inverse distance transform mapping is formed. This map can have multiple centers as references for distance mapping. Different weights can be assigned to different centers. Then the map, scaled between 0 and 1, will serve as a template, which means to get the final 4D enhancement pattern, the mapping template will need to be multiplied by the current 4D phantom at any time point. Equation 12 describes the inverse distance mapping mathematically as follows.

$$Temp(x,y,z) = [1 - \sum\nolimits_{i=1}^{i=n} W_i \cdot exp(-\frac{\sqrt{((x-x_i)^2 + (y-y_i)^2 + (z-z_i)^2)}}{S_i^2})] \tag{12}$$

Where the x_i, y_i, z_i are the center of the necrotic core. Multiple centers can be chosen to mimic irregular necrotic core, as long as the total weight sum to 1 as described by equation 13.

$$\sum\nolimits_{i=1}^{i=n} W_i = 1 \tag{13}$$

All the weight W_i are positive numbers between 0 and 1. A necrotic core effect is displayed in the following Figure 19. The total number of centers are each chosen to be 1, 3, 6. We can see that with multiple centers, differnt shapes of the necrotic core can be modeled. Only the central slice at a given time slice is displayed in the figure.

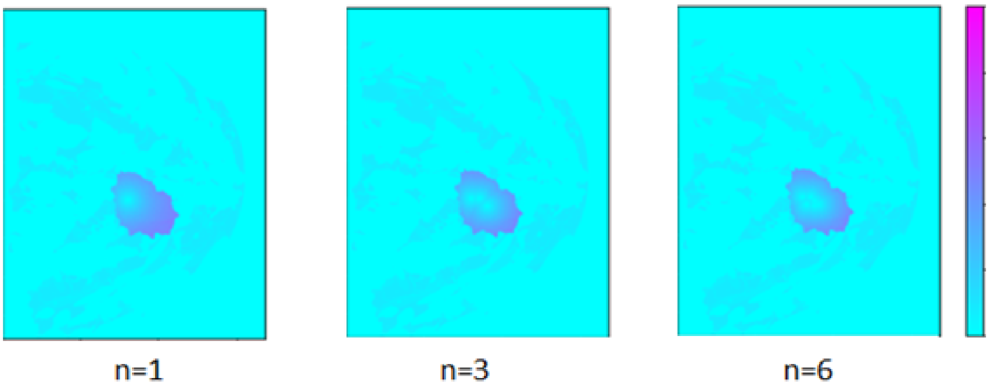

Figure 19: The total number of centers are each chosen to be 1, 3, 6.

When the number of centers exceeds a certain number, for example, one or multiple enclosed areas are specified to be the withered center, another approach will be used for the necrotic core simulation. Instead of calculating all the exponents for each center in equation 12, we find the nearest center for each voxel and use the Euclidean distance as the single exponent in the following equation 14. The model adopted here is similar to the one in the previous delay map section. As for the enclosed dead hollow core, to allow for an irregular shape, a Gaussian random sphere is utilized to simulate the hollow core.

$$Temp(x, y, z) = [1 - exp(-\frac{\sqrt{((x - x_i)^2 + (y - y_i)^2 + (z - z_i)^2)}}{S^2})] \tag{14}$$

Where the index i for the specific artery voxel ID is chosen such that it has the smallest Euclidean distance to the voxel of interest.

$$i = \arg\min_i \sqrt{((x - x_i)^2 + (y - y_i)^2 + (z - z_i)^2)} \tag{15}$$

Following Figure 20 is a necrotic mass with hollow core.

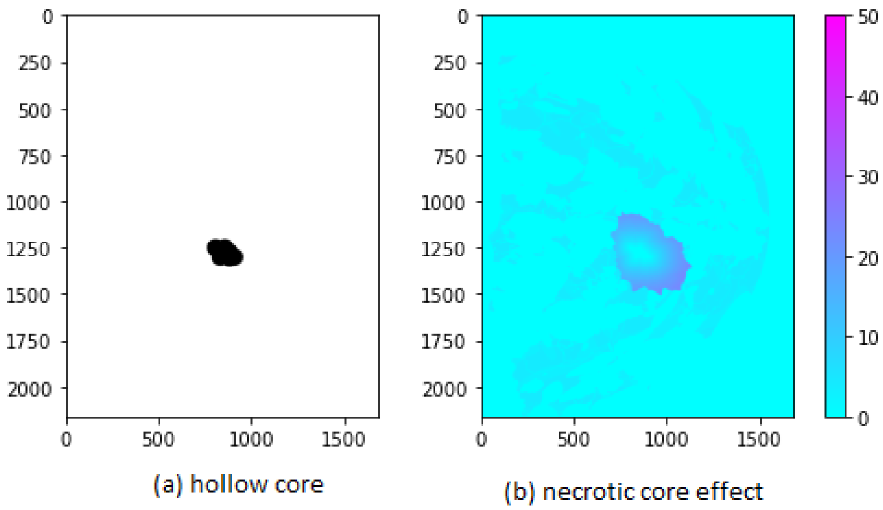

Figure 20: Left side is the hollow core inserted, right side is the final necrotic core effect.

3 Simulation of a mammogram using the Monte Carlo method

A Monte Carlo simulation is a statistical probabilistic approach to developing experiments or simulations to investigate the nondeterministic probability distribution of inputs and outcomes. Compared to the direct ray-tracing method, it provides the potential for a more realistic result by simulating the interaction between billions of photons and tissues according to the photon spectra and cross-section interaction characteristics.

The mammogram in this work is simulated using the MC-GPU Monte Carlo method developed by Andreu Badal[8]. It was made available through Github. According to the author, this MC-GPU method was developed specifically to simulate a Siemens Mammomat Inspiration system for the Virtual Imaging Clinical Trial for Regulatory Evaluation (VICTRE) project.

The software employs PENELOPE's well-known x-ray-matter interaction physics and material-specific interaction cross-sections. A huge number of x-ray tracks from the source to the detector via the patient are simulated, and the average amount of energy deposited in each tissue of the patient and the average signal created in each pixel of the detector are tallied. Due to the fact that each x-ray track is independent of the others, MC-GPU uses the CUDA library to simulate the tracks in parallel across thousands of processing cores of a Graphics Processing Unit (GPU). Considering the scale of the simulation, a typical simulation of a mammogram requires at least billions of photons generated, GPU's parallel computation reduced the time needed for the simulation drastically.

The goal of the MC-GPU program development was to produce models that were as realistic as possible from basic physical principles, the use of fitting parameters or approximations is not utilized since it could jeopardize the validity of the simulation findings or possibly limit its application. Compared to other x-ray imaging modeling methods, such as simple ray-tracing with exponential attenuation, the Monte Carlo algorithm accurately simulates the primary beam and scattering contributions to images, quantum noise, extended focal spot, patient dose, depth-of-interaction effects in the detector response at angular incidence, and other relevant phenomena. A mammogram generated using this MC-GPU code is displayed in Figure 21.

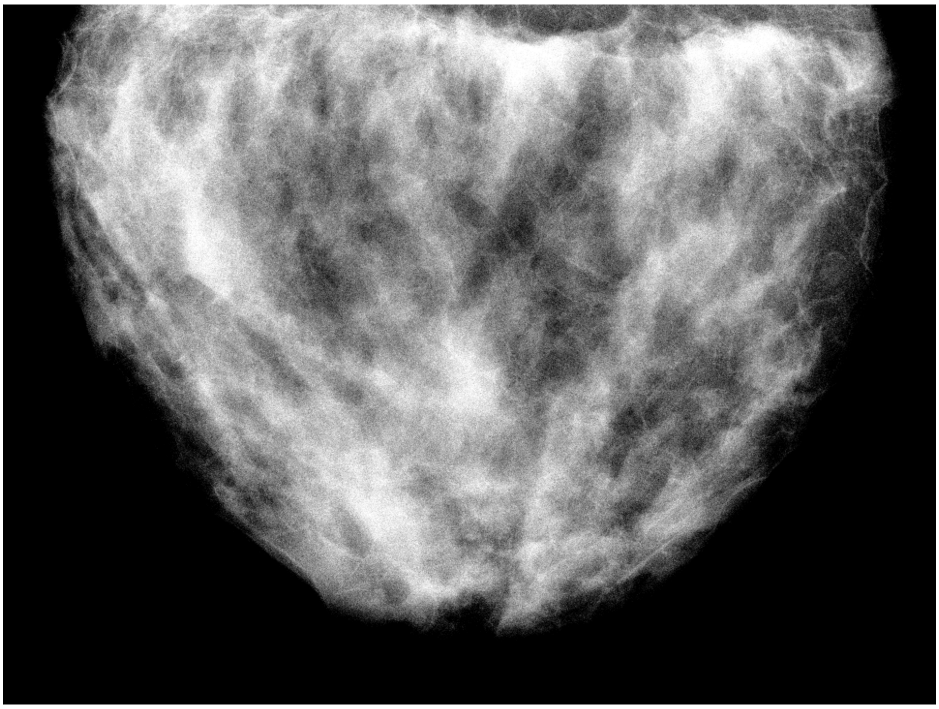

Figure 21: A mammogram generated using the MC-GPU method.

To use the MC-GPU software, multiple parameters need to be specified, which include the energy spectra, number of photons simulated, 3D phantom with voxel values indicating different tissues, and mean free path values for all sorts of cross-sections of each tissue type(also known as material files in the software). The last one, material files of different tissues, is a little bit tricky in our case due to the varied iodine mixture present in the blood.

3.1 Material files

Two steps are taken to allow varied iodine blood mixture material files (here we used iodine to represent the contrast agent). First, discretization needs to be performed to properly represent the limited number of materials. While the software in default sets 15 as the maximum number of materials, the parameter can be changed to a higher value. It is not recommended to have a large number of material files, so here we set the maximum number of materials to be 65. The iodine blood tissue mixture is discretized differently for different tissues. For iodine blood mass tissue mixture, due to a large range of the iodine uptake level, 40 bins are made between 0 mg/ml and 10 mg/ml. As for iodine blood fibro glandular tissue mixture, 5 bins are made between 0 mg/ml and 0.2 mg/ml. Those two ranges specified above cover the peak value of the relevant time enhancement curves.

The second step is to calculate the mean free path values of all sorts of cross-sections. Here a linear combination approach is used. With the material files of mass tissue, fibro glandular tissue, blood, and iodine contrast agent, equation 16 is used to compute the mean free paths of different cross-sections. The material files of mass, fibro glandular tissue, blood, and iodine are each generated using the Penelope method according to a previous literature[9]

$$1/d_m = P_t/d_t + (1 - P_t)/(P_{c,t}/d_c + (1 - P_{c,t})/d_b) \tag{16}$$

Here d_m, d_t, d_c, d_b are each referring to the mean free paths for mixture material, tissue(fibro glandular or mass tissue), contrast agent(iodine) and blood. P_t refers to the weight fraction of the tissue mixture made of tissue t. For fibro glandular tissue, P_t is modeled as 0.8, while 0.6 is assigned for mass tissue weight fraction. Similarly, $P_{c,t}$ is the weight fraction of the contrast agent in the contrast agent-blood mixture in tissue t. This value can be calculated using the density of blood, the concentration level of iodine, and the density of iodine.

The previous equation 16 might be easier to read if all of the mean free path values are replaced by the attenuation coefficients. the linear combination pattern is easier to spot in equation 17.

$$\mu_m = P_t \cdot \mu_t + (1 - P_t) \cdot (P_{c,t} \cdot \mu_c + (1 - P_{c,t}) \cdot \mu_b) \tag{17}$$

3.2 Simulation result

Given all the previously established information, mammograms can be simulated and displayed as following Figure 22. Here we can see with the iodinated contrast agent, it is easier to spot the mass. The 50s figure models the peak of the concentration of the contrast agent, which gives a good contrast. The 5s figure does not have a good contrast due to the low concentration of the iodine.

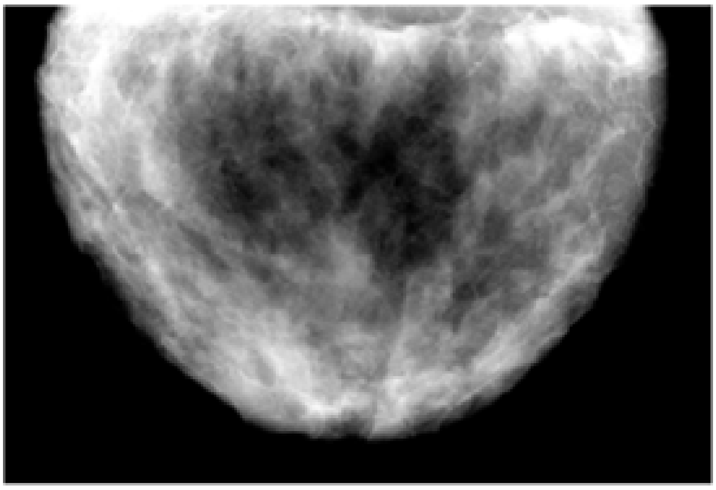

49 KVP 5S

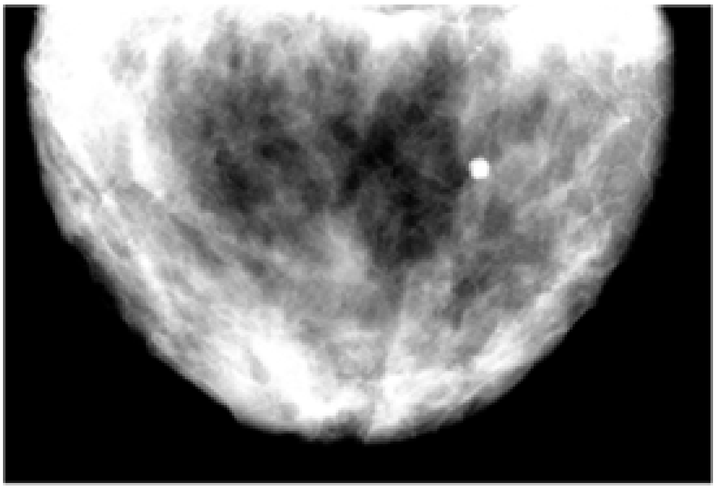

49KVP 50S

Figure 22: 50s figure models the peak of the concentration of contrast agent, which gives a good contrast. 5s figure does not have a good contrast due to the low concentration of the iodine.

4 Contrast-Enhanced Imaging

In this chapter, contrast-enhanced digital mammography (CEDM) was utilized to form a two-dimensional contrast enhancement map of the breast, which has a great potential to help identify the neovasculature of breast cancer and hence increase the cancer detection and classification rates. CEDM has been proven in multiple studies to be superior to full-field digital mammography (FFDM) and comparable to dynamic contrast-enhanced magnetic resonance imaging(DCE-MRI). Here we use this technique to explore the benefit of the 4D phantom .

4.1 CEDM foundation

There are multiple algorithms to achieve contrast enhanced mammograms, the method[10]realized here is to generate the image via log scale weighted subtraction between high energy and low energy mammograms as described by the following equation 19

$$DE = log(HE) - log(LE) \cdot w \tag{18}$$

$$DE = -log(HE/blank_H) + log(LE/blank_L) \cdot w \tag{19}$$

W is the weighting factor, it varies with different energy spectra and different breast densities. The value of w is computed by an analytical model that simulates the imaging system and the breast.

According to previous studies[11][12], the x-ray spectra were produced at 26 to 33 kVp and 49 kVp using the tungsten anode spectral model described by Boone, where the breast was modeled as a simplified object made up of glandular and adipose tissue. The density of glandular tissue ranges from 0% to 100% while discretization is done with 10% spacing, and the thickness of the breasts ranges from 0 to 10 cm at 0.5 cm space. The detector was modeled as a 300-m a-Se conversion layer energy-integrating detector. The signal intensities under various x-ray beam qualities for varying breast attenuation were determined using this analytical model. With the signal intensity of high energy and low energy in log scale, a linear regression can be applied for certain breast density and energy spectra. The weighting factor w can be specified by the slope of the linear regression.

4.2 Contrast Enhanced Imaging result

In this work, 27kvp is used for the low energy spectra, 49 kvp for the high energy spectra. According to the plot from Hailiang Huang's work, the weighting factor w is about 0.237 for 4cm breast thickness.

We can see from figure 23, that the small mass inserted in the right-up corner is quite hard to spot. Among four mammograms, only through one of them, the mass in the right-upper quadrant can be observed easily. For this mammogram, the spectra energy used here is 49kvp, which provides good contrast between iodinated contrast agent and tissues. The phantom used for this mammogram also models a malignant tumor at the peak of its contrast agent concentration at 50s time slice. Those two criteria together create a good contrast between the mass and the surrounding tissues. For other mammograms, it is quite hard to spot the mass without the timing and energy spectra criteria.

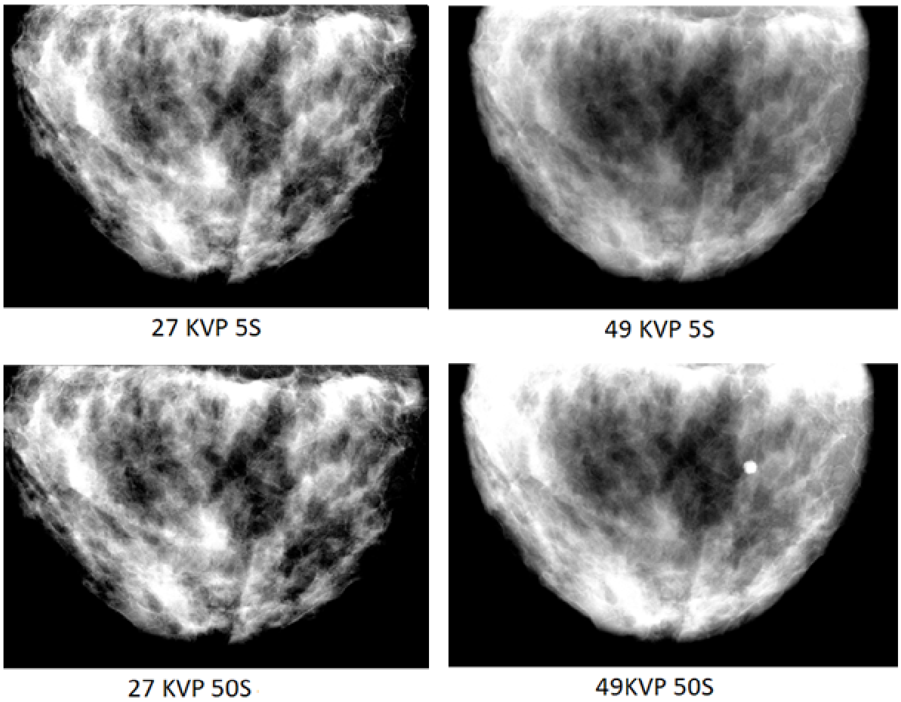

Figure 23: mammograms generated using the multiple energy spectra and 4D phantom at different time points.

After processing the mammograms with the log scale subtraction method, according to figure 24, we can spot the mass easily from multiple time points.

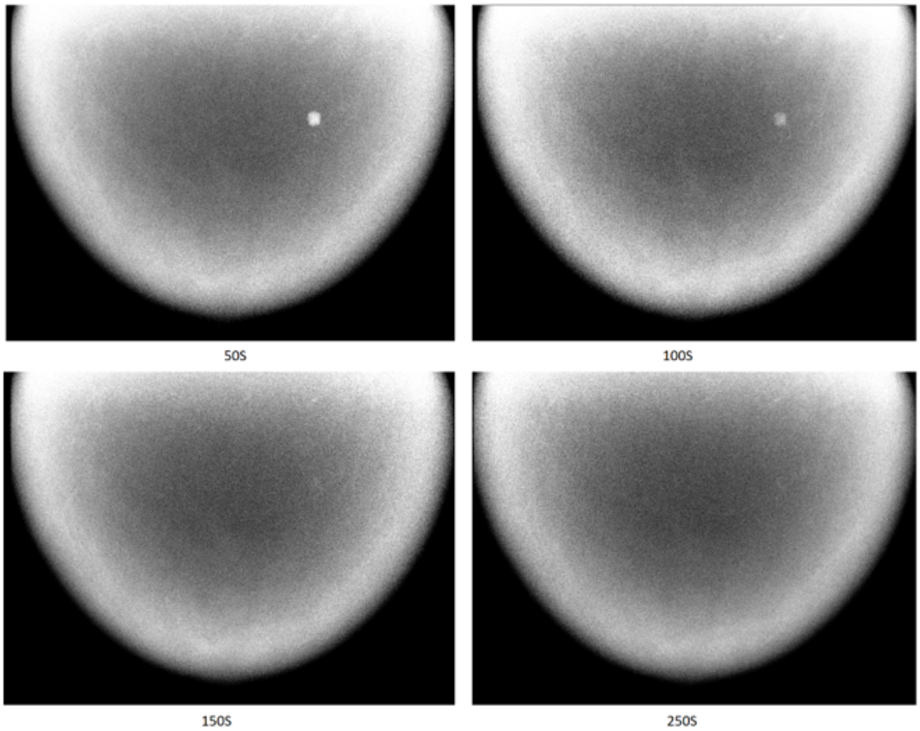

Figure 24: Contrast enhanced mammogram at differnt time point of the 4D phantom.

5 Conclusions

The 4D digital breast phantom models multiple features for the simulation of breast imaging. Since a major challenge in the field of cancer detection lies in the differentiation between fibro glandular tissue and different mass tissues, the diffusion processes of fibro glandular tissue and different types of mass tissues are focused on in this work. Physical parameters like wash-in and wash-out rates are employed to simulate the diffusion process of mass, which allows different characteristics of mass. In addition to that, Gaussian random sphere and inverse distance mapping are constructed to mimic the irregularity of the necrotic core.

To explore the benefit of the 4D phantom, digital mammograms are simulated and studied by the Monte Carlo method. To perform the simulation, the contrast agent blood tissue mixture's cross-section parameters are generated by linear interpolation between the parameters of blood, contrast agent, and tissue(mass or fibro glandular tissue). With the contrast agent in the tissue, higher contrast is achieved between fibro glandular tissue and mass tissue. The contrast is then further enhanced by the log scale subtraction between high and low-energy mammograms.

Future work will expand to the analysis of DBT and CT based on this 4D phantom. Another approach, for example using Penelope directly, for the mixture material's cross-section parameters can be explored. A physical phantom of the breast containing contrast agent can also be fabricated with the help of this work[13][14]. Other display approaches, for example, Houdini, are being explored to present the 4D phantom better.

References

[1] Caballo, M., Mann, R., and Sechopoulos, I., "Patient-based 4d digital breast phantom for perfusion contrast-enhanced breast ct imaging," *Medical physics* **45**(10), 4448–4460 (2018).

[2] Graff, C. G., "A new, open-source, multi-modality digital breast phantom," in [*Medical Imaging 2016: Physics of Medical Imaging*], **9783**, 72–81, SPIE (2016).

[3] De Sisternes, L., Brankov, J. G., Zysk, A. M., Schmidt, R. A., Nishikawa, R. M., and Wernick, M. N., "A computational model to generate simulated three-dimensional breast masses," *Medical physics* **42**(2), 1098–1118 (2015).

[4] Klarhöfer, M., Csapo, B., Balassy, C., Szeles, J., and Moser, E., "High-resolution blood flow velocity measurements in the human finger," *Magnetic Resonance in Medicine: An Official Journal of the International Society for Magnetic Resonance in Medicine* **45**(4), 716–719 (2001).

[5] Geddes, D. T., Aljazaf, K. M., Kent, J. C., Prime, D. K., Spatz, D. L., Garbin, C. P., Lai, C. T., and Hartmann, P. E., "Blood flow characteristics of the human lactating breast," *Journal of Human Lactation* **28**(2), 145–152 (2012).

[6] Ricci, P., Cantisani, V., Ballesio, L., Pagliara, E., Sallusti, E., Drudi, F., Trippa, F., Calascibetta, F., Erturk, S., Modesti, M., et al., "Benign and malignant breast lesions: efficacy of real time contrast-enhanced

ultrasound vs. magnetic resonance imaging," *Ultraschall in der Medizin-European Journal of Ultrasound* **28**(01), 57–62 (2007).

[7] Ellner, S. P. and Guckenheimer, J., "Dynamic models in biology," in [*Dynamic Models in Biology*], Princeton University Press (2011).

[8] Badal, A. and Badano, A., "Accelerating monte carlo simulations of photon transport in a voxelized geometry using a massively parallel graphics processing unit," *Medical physics* **36**(11), 4878–4880 (2009).

[9] Kiarashi, N., Lo, J. Y., Lin, Y., Ikejimba, L. C., Ghate, S. V., Nolte, L. W., Dobbins, J. T., Segars, W. P., and Samei, E., "Development and application of a suite of 4-d virtual breast phantoms for optimization and evaluation of breast imaging systems," *IEEE transactions on medical imaging* **33**(7), 1401–1409 (2014).

[10] Huang, H., Scaduto, D. A., Liu, C., Yang, J., Zhu, C., Rinaldi, K., Eisenberg, J., Liu, J., Hoernig, M., Wicklein, J., et al., "Comparison of contrast-enhanced digital mammography and contrast-enhanced digital breast tomosynthesis for lesion assessment," *Journal of medical imaging* **6**(3), 031407 (2019).

[11] Boone, J. M. and Seibert, J. A., "An accurate method for computer-generating tungsten anode x-ray spectra from 30 to 140 kv," *Medical physics* **24**(11), 1661–1670 (1997).

[12] Boone, J. M., Fewell, T. R., and Jennings, R. J., "Molybdenum, rhodium, and tungsten anode spectral models using interpolating poly-

nomials with application to mammography," *Medical physics* **24**(12), 1863–1874 (1997).

[13] Ikejimba, L. C., Glick, S. J., Choudhury, K. R., Samei, E., and Lo, J. Y., "Assessing task performance in ffdm, dbt, and synthetic mammography using uniform and anthropomorphic physical phantoms," *Medical physics* **43**(10), 5593–5602 (2016).

[14] Ikejimba, L. C., Salad, J., Graff, C. G., Goodsitt, M., Chan, H.-P., Huang, H., Zhao, W., Ghammraoui, B., Lo, J. Y., and Glick, S. J., "Assessment of task-based performance from five clinical dbt systems using an anthropomorphic breast phantom," *Medical physics* **48**(3), 1026–1038 (2021).